



Bursting oscillations with boundary homoclinic bifurcations in a Filippov-type Chua's circuit

ZHIXIANG WANG^{1,2}, CHUN ZHANG², ZHENGDI ZHANG³ and QINSHENG BI^{1,*}

¹Faculty of Civil Engineering and Mechanics, Jiangsu University, Zhenjiang 212013, China

²School of Mathematics and Statistics, Huaiyin Normal University, Huai'an 223300, China

³Faculty of Science, Jiangsu University, Zhenjiang 212013, China

*Corresponding author. E-mail: qshengb@126.com

MS received 20 December 2019; revised 5 April 2020; accepted 22 April 2020;
published online 2 July 2020

Abstract. A modified version of the typical Chua's circuit, which possesses a periodic external excitation and a piecewise nonlinear resistor, is considered to investigate the possible bursting oscillations and the dynamical mechanism in the Filippov system. Two new symmetric periodic bursting oscillations are observed when the frequency of external excitation is far less than the natural one. Besides the conventional Hopf bifurcation, two non-smooth bifurcations, i.e., boundary homoclinic bifurcation and non-smooth fold limit cycle bifurcation, are discussed when the whole excitation term is regarded as a bifurcation parameter. The sliding solution of the Filippov system and pseudo-equilibrium bifurcation of the sliding vector field on the switching manifold are analysed theoretically. Based on the analysis of the bifurcations and the sliding solution, the dynamical mechanism of the bursting oscillations is revealed. The external excitation plays an important role in generating bursting oscillations. That is, bursting oscillations may be formed only if the excitation term passes through the boundary homoclinic bifurcation. Otherwise, they do not occur. In addition, the time intervals between two symmetric adjacent spikes of the bursting oscillations and the duration of the system staying at the stable pseudonode are dependent on the excitation frequency.

Keywords. Filippov system; periodic external excitation; non-smooth bifurcation; bursting oscillations.

PACS Nos 05.45.–a; 05.45.Pq; 05.45.Xt

1. Introduction

Bursting oscillations belong to the class of mixed-mode oscillations, which may occur in the slow–fast dynamical system [1]. This phenomenon is ubiquitous in physics [2], chemistry [3], biochemistry [4] and neuroscience [5–7]. The generation mechanism of bursting oscillations of slow–fast system has been understood thanks to the slow–fast analysis method introduced by Rinzel [8]. Subsequent to this pioneering work, Izhikevich [9] summarised the bifurcation mechanism of bursting oscillations and classified almost all the bursting oscillations in low-dimensional systems. Bursting oscillations may occur in a non-autonomous system with periodic external excitation under the condition that the external excitation has a low frequency. Such a system can be treated as a slow–fast system by regarding the whole excitation term as a slow-varying variable. In this case, a powerful tool, termed ‘transformed

phase diagram’, is introduced to explain the dynamical mechanism of the bursting oscillations [10]. Up to now, most of the literatures on bursting oscillations are confined to smooth or piecewise smooth continuous dynamical systems (e.g. [11–15] and references therein).

A Filippov system is a piecewise discontinuous system. It usually has one or more discontinuity boundaries (switching manifolds) which may cause qualitative changes in a system's dynamics, termed discontinuity-induced bifurcations or non-smooth bifurcations. They include boundary equilibrium bifurcations occurring when an equilibrium meets a switching manifold. They also include sliding bifurcations occurring when an attracting periodic orbit meets a switching manifold, thereby loses or gains a segment of sliding [16]. Bursting behaviours may occur when a Filippov system involves slow-varying and fast-varying variables. The existence of non-smooth bifurcations in the Filippov

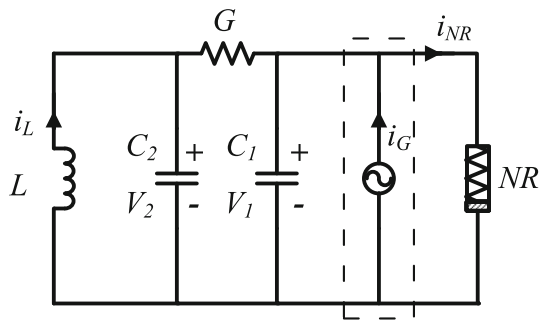


Figure 1. The modified Chua's circuit.

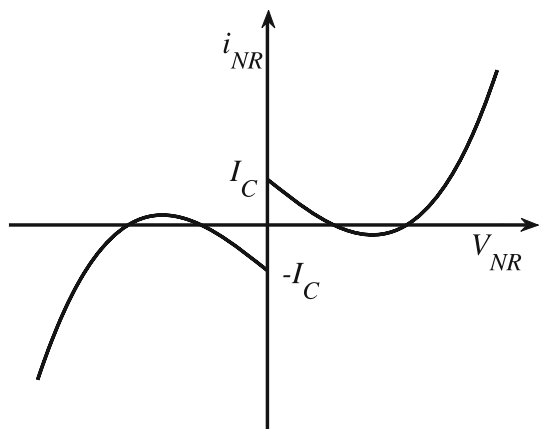


Figure 2. The $i-v$ characteristic curve of the nonlinear resistor NR .

system may lead to complicated bursting patterns. Thus, investigating the bursting oscillations in the Filippov system and accounting for the dynamical mechanism have attracted many scholars' attention [17,18]. However, up to now, the effects of boundary homoclinic bifurcation, non-smooth fold limit cycle bifurcation and the sliding vector field on the bursting dynamics were rarely reported in the published papers we have read.

Chua's circuit, which is a well-known generator of chaotic oscillations, has not only become one of the most common examples in research articles on nonlinear oscillation [19], but has also been used in secret communication [20] and voice encryption [21]. A very simple modification of a scheme can lead to substantial new results [22,23].

In this paper, we investigate the dynamical mechanism of bursting oscillations in three-dimensional Filippov system, focussing on the effects of boundary homoclinic bifurcation, non-smooth fold limit cycle bifurcation and the sliding vector field on the bursting dynamics. For this purpose, the typical Chua's circuit is modified, which is shown in figure 1, where i_G is a periodically exciting current and NR is a non-linear resistor whose $i-v$ characteristic curve is piecewise and cubic (see figure 2).

2. Mathematical model and its bursting oscillations

The equations of the circuit are

$$\begin{aligned} C_1 \frac{dV_1}{d\tau} &= G(V_2 - V_1) - g(V_1) + I_G \sin(\omega\tau), \\ C_2 \frac{dV_2}{d\tau} &= G(V_1 - V_2) + i_L, \\ L \frac{di_L}{d\tau} &= -V_2, \end{aligned} \tag{1}$$

where

$$g(V_1) = \begin{cases} -G_A V_1 + G_B V_1^3 + I_C, & \text{if } V_1 > 0, \\ -G_A V_1 + G_B V_1^3 - I_C, & \text{if } V_1 < 0, \end{cases} \tag{2}$$

corresponding to figure 2, denotes the relationship between the current and voltage passing across NR , G_A and G_B are conductance and I_C is a direct current. We assume $G \neq G_A$ in this paper. The system is governed by different differential equations when $V_1 > 0$ or $V_1 < 0$. Therefore, $H(V_1, V_2, i_L) = V_1 = 0$ is a switching surface.

By applying the following changes of variables: $V_1 = (I_C/G)x$, $V_2 = (I_C/G)y$, $i_L = I_Cz$ and $\tau = (C_2/G)t$, (1) can be normalised and rewritten in the dimensionless form

$$\dot{\mathbf{x}} = \begin{cases} f^+(\mathbf{x}, w) = (f_1^+, f_2^+, f_3^+), & \text{if } x > 0, \\ f^-(\mathbf{x}, w) = (f_1^-, f_2^-, f_3^-), & \text{if } x < 0, \end{cases} \tag{3}$$

where

$$f^+(\mathbf{x}, w) = (\alpha(y + (a - 1)x - bx^3 - 1) + w, x - y + z, -\beta y), \tag{4}$$

$$f^-(\mathbf{x}, w) = (\alpha(y + (a - 1)x - bx^3 + 1) + w, x - y + z, -\beta y), \tag{5}$$

with

$$\begin{aligned} \mathbf{x} &= (x, y, z) \in R^3, \quad \alpha = \frac{C_2}{C_1}, \quad \beta = \frac{C_2}{LG^2}, \\ a &= \frac{G_A}{G}, \quad b = \frac{G_B I_C^2}{G^3}, \quad \gamma = \frac{C_2 I_G}{C_1 I_C}, \quad \Omega = \frac{\omega C_2}{G} \end{aligned}$$

and

$$w = \gamma \sin(\Omega t),$$

satisfying the conditions $\alpha > 0, \beta > 0, \gamma > 0, \omega > 0, a > 0, b > 0$ and $a \neq 1$.

The switching surface is redefined as $h(x, y, z) = x = 0$, and the switching manifold is written as $\Sigma = \{\mathbf{x} | x = 0\}$. Σ divides the phase space into two subregions, denoted by Σ_{\pm} with $\Sigma_+ = \{\mathbf{x} \in R^3 | x > 0\}$ and $\Sigma_- = \{\mathbf{x} \in R^3 | x < 0\}$, respectively. Obviously, the dynamics of the system in Σ_{\pm} are governed by $\dot{\mathbf{x}} = f^{\pm}(\mathbf{x}, w)$, respectively.

If $0 < \Omega \ll 1$, there may exist an order gap between the excitation frequency Ω and the natural one Ω_N ,

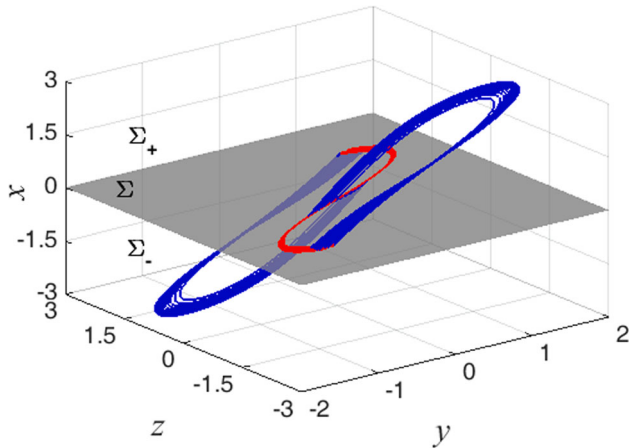


Figure 3. Three-dimensional phase portrait of the bursting oscillations for $\gamma = 3.0$, where the blue segments are in the regions Σ_{\pm} and the red segments are on the switching manifold Σ .

implying that system (3) is a slow–fast system and Ω may satisfy $0 < \Omega \ll \Omega_N$, in which $w = \gamma \sin(\Omega t)$ is the slow subsystem. In this case, during an arbitrary period $2\pi/\Omega_N$, i.e., $t \in [t_0, t_0 + (2\pi/\Omega_N)]$, the excitation term w varies between $w_0 = \gamma \sin(\Omega t_0)$ and $w_N = \gamma \sin(\Omega t_0 + 2\pi(\Omega/\Omega_N))$, implying $w_0 \approx w_N$. As state variables may oscillate mainly according to the natural frequency Ω_N , the analysis above means that w keeps almost a constant value during any arbitrary oscillating period [24]. Therefore, w can be regarded as a bifurcation parameter to explore the bifurcation mechanism of bursting oscillations.

When the parameters are fixed at $a = 0.95$, $b = 0.1$, $\alpha = 1.82$, $\beta = 0.23$ and $\Omega = 0.005$, two types of new bursting oscillations can be observed with the variation of the excitation amplitude. Here, the initial values of the state variables are set at $x_0 = 0.1$, $y_0 = 0.1$ and $z_0 = 0.1$.

Numerical simulation shows that bursting oscillations do not occur if γ is less than some critical value γ_0 . If $\gamma > \gamma_0$, bursting oscillations appear. For a typical case, when $\gamma = 3.0$, the bursting oscillations are shown in figures 3–6.

When γ is larger than γ_0 and less than another critical value γ_1 , the system keeps similar bursting patterns as above. If $\gamma > \gamma_1$, new bifurcations involve the bursting attractor, forming new bursting oscillations (see the representative ones in figure 7–10 for $\gamma = 3.8$).

Remark 1. According to §3.4, the critical value $\gamma_0 = \alpha = 1.82$, and the critical value $\gamma_1 \approx 3.254$.

In order to explore the mechanism of the bursting oscillations, in the following section, we turn to the bifurcation analysis of the non-smooth vector field.

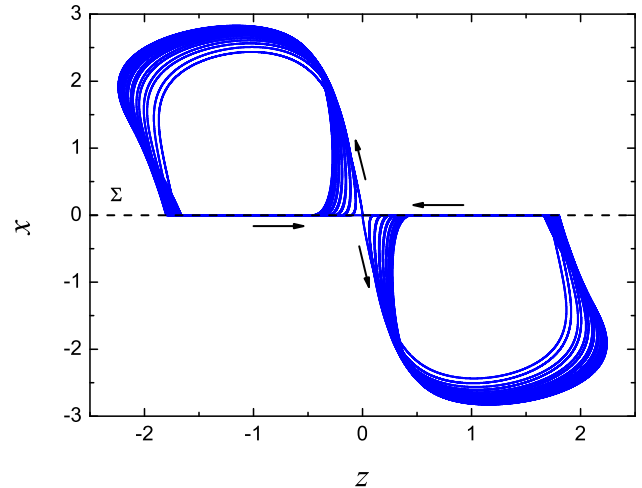


Figure 4. Phase portrait of the bursting oscillations on the (z, x) plane for $\gamma = 3.0$.

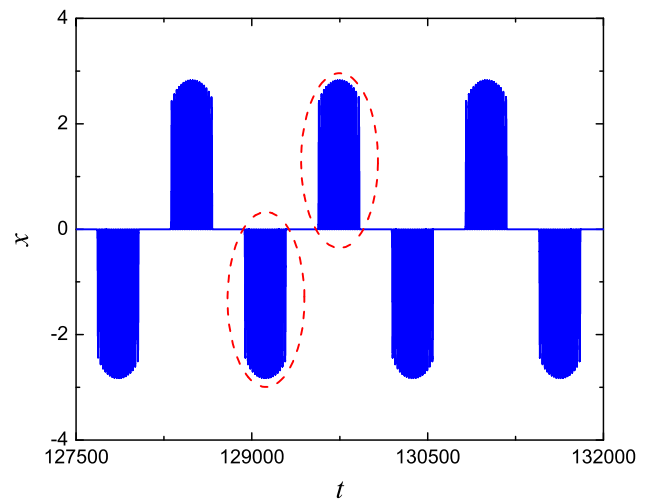


Figure 5. Time history of the bursting oscillations on the (t, x) plane for $\gamma = 3.0$.

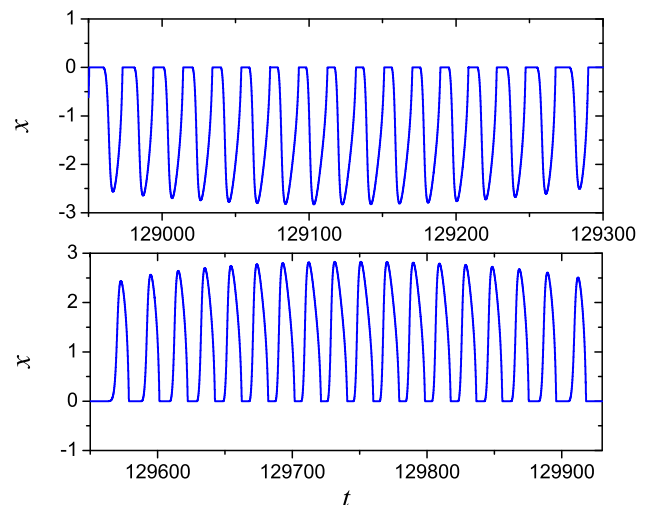


Figure 6. Locally enlarged parts of figure 5.

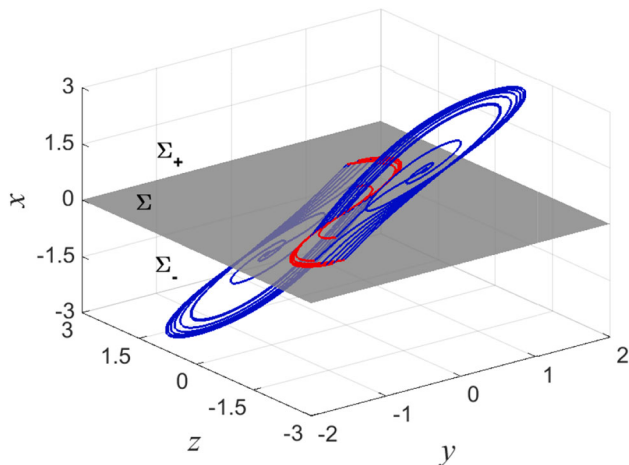


Figure 7. Three-dimensional phase portrait of the bursting oscillations for $\gamma = 3.8$, where the blue segments are in the regions Σ_{\pm} and the red segments are on the switching manifold Σ .

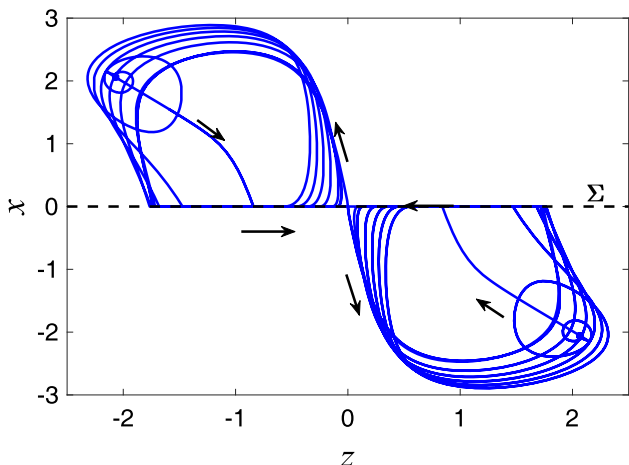


Figure 8. Phase portrait of the bursting oscillations on the (z, x) plane for $\gamma = 3.8$.

3. Bifurcation analysis

3.1 Pseudoequilibrium analysis and sliding solution on the switching manifold

The switching manifold Σ partitions the phase space into two subregions Σ_{\pm} . The directional Lie derivatives

$$L_{f_{\pm}}h = \langle \nabla h, f^{\pm}(\mathbf{x}, w) \rangle = f_1^{\pm} \quad (6)$$

determine the kind of contact of smooth vectors $f^{\pm}(\mathbf{x}, w)$ with Σ , where $h = x$, ∇h and $\langle \cdot, \cdot \rangle$ denote the gradient of smooth function h and the canonical inner product, respectively [25].

If $L_{f_{\pm}}h = 0$, we get two sets of tangential singularities $S^{\pm} = \{\mathbf{x} \in \Sigma | f_1^{\pm} = 0\} = \{\mathbf{x} \in \Sigma | \alpha(y \mp 1) + w = 0\}$, which divide the switching manifold Σ into three

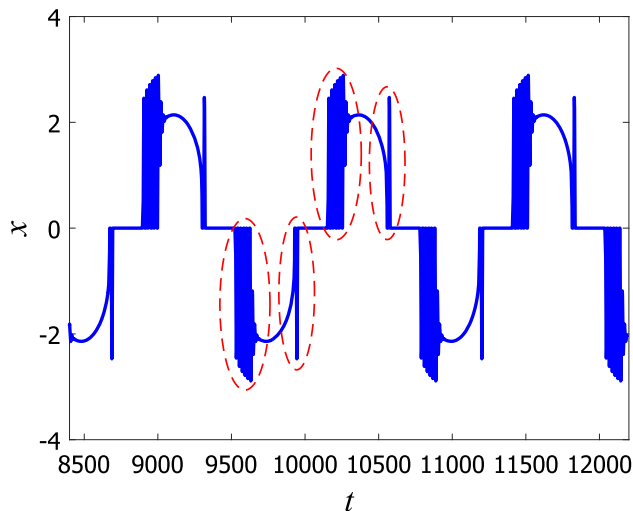


Figure 9. Time history of the bursting oscillations on the (t, x) plane for $\gamma = 3.8$.

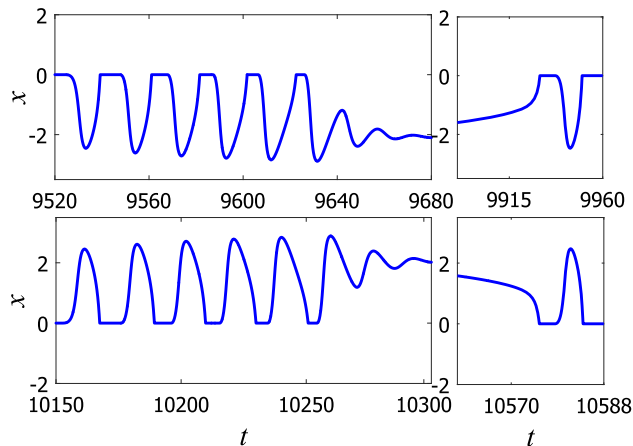


Figure 10. Locally enlarged parts of figure 9.

subregions, denoted by $\Sigma^{c\pm}$ and Σ^s with $\Sigma^{c+} = \{\mathbf{x} \in \Sigma | f_1^+ > 0, f_1^- > 0\}$, $\Sigma^{c-} = \{\mathbf{x} \in \Sigma | f_1^+ < 0, f_1^- < 0\}$ and $\Sigma^s = \{\mathbf{x} \in \Sigma | f_1^+ < 0, f_1^- > 0\}$, respectively. $\Sigma^{c\pm}$ and Σ^s are termed crossing regions and sliding region, respectively.

S^{\pm} are a pair of parallel lines with respect to w and y on Σ if the parameter α is fixed, and the distance between S^+ and S^- is 2. In other words, the shape of the sliding region Σ^s remains unchanged during the variation of the parameter w , while their position changes on Σ . A diagrammatic sketch of the three subregions and two sets of tangential singularities are shown in figure 11.

When $\mathbf{x} \in \Sigma^s$, following the Filippov convention (see [26]), the sliding vector field associated with $f^+(\mathbf{x}, w)$ and $f^-(\mathbf{x}, w)$ is the vector field $\hat{f}^s(\mathbf{x})$ which is tangent to Σ and expressed in coordinates as

$$\hat{f}^s(\mathbf{x}) = (1 - \delta)f^+(\mathbf{x}, w) + \delta f^-(\mathbf{x}, w), \quad (7)$$

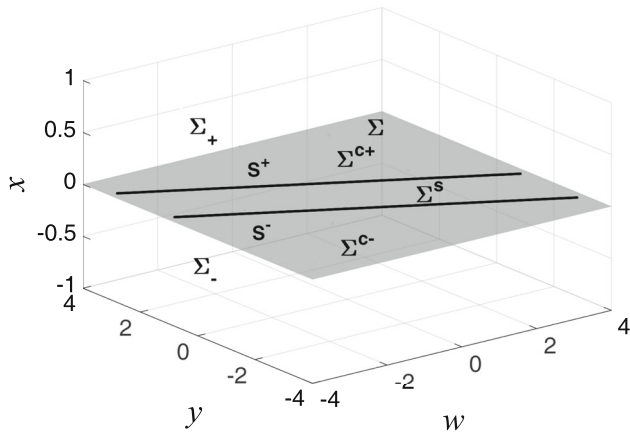


Figure 11. Diagrammatic sketch of the three subregions and the two sets of tangent singularities for $\alpha = 1.82$.

where

$$\delta = \frac{L_{f+h}}{L_{f+h} - L_{f-h}}.$$

A straightforward calculation gives

$$\hat{f}^s(\mathbf{x}) = (0, -y + z, -\beta y). \tag{8}$$

Note that, in the region Σ^s , system $\dot{\mathbf{x}} = \hat{f}^s(\mathbf{x})$ is topologically equivalent [25] to

$$\dot{x}^s = f^s(y, z) = (-y + z, -\beta y), \tag{9}$$

where $x^s = (y, z) \in \Sigma$. We can take advantage of the invariance of Σ under the flow determined by f^s and reduce the dimension of the problem by one.

When $\hat{f}^s(\mathbf{x}) = 0$, we get the pseudoequilibrium of (3) at $E_s = (0, 0, 0)$. The stability of E_s is equivalent to that of $E_0 = (0, 0)$ which is the equilibrium of (9). The stability of E_0 can be determined by the eigenvalues of the associated Jacobian matrix $(df^s(y, z)/dx^s)|_{E_0}$, which are

$$\lambda_{1,2} = \frac{-1 \pm \sqrt{1 - 4\beta}}{2}.$$

This means that E_s is a stable pseudonode or a stable pseudofocus, and so there is no bifurcation associated with the pseudoequilibrium of the sliding vector field.

The analytical solution of (9) can be written as

$$\begin{aligned} y &= y(t) = c_1 \exp(\lambda_1 t) + c_2 \exp(\lambda_2 t), \\ z &= z(t) = (\lambda_1/\beta)c_1 \exp(\lambda_2 t) + (\lambda_2/\beta)c_2 \exp(\lambda_1 t), \end{aligned} \tag{10}$$

for $\beta \neq \frac{1}{4}$ or

$$\begin{aligned} y &= y(t) = (c_1 + c_2 t) \exp\left(-\frac{1}{2}t\right), \\ z &= z(t) = (-2c_1 t - c_2 t^2) \exp\left(-\frac{1}{2}t\right), \end{aligned} \tag{11}$$

for $\beta = \frac{1}{4}$, where c_1 and c_2 are two constants which are determined by the initial conditions of (9). Equation (10) or (11) can describe the route from the point, which is the intersection of the trajectory and Σ , to the stable pseudonode or stable pseudofocus.

3.2 Equilibrium analysis of the fast subsystem

Now we turn to the bifurcation analysis of the fast subsystems by regarding the whole excitation term $\omega = \gamma \sin(\Omega t)$ as a bifurcation parameter.

The admissible equilibria of the subsystems $\dot{x} = f^\pm(\mathbf{x}, w)$ can be computed at $E_\pm = (X_\pm, 0, -X_\pm)$, where $\text{sign}(X_\pm) = \pm 1$ and X_\pm satisfy

$$\alpha((a - 1)X_\pm - bX_\pm^3 \mp 1) + w = 0, \tag{12}$$

respectively. The stability of the equilibria E_\pm can be determined by the associated characteristic equations, written in the form

$$\lambda^3 + Q_{1\pm}\lambda^2 + Q_{2\pm}\lambda + Q_{3\pm} = 0, \tag{13}$$

respectively, where $Q_{1\pm} = 3\alpha bX_\pm^2 - a\alpha + \alpha + 1$, $Q_{2\pm} = 3\alpha bX_\pm^2 - a\alpha + \beta$, $Q_{3\pm} = 3\alpha b\beta X_\pm^2 - a\alpha\beta + \alpha\beta$. Fold bifurcation of the equilibrium point may be observed if

$$3\alpha b\beta X_\pm^2 - a\alpha\beta + \alpha\beta = 0, \tag{14}$$

and $Q_{1\pm} > 0$, $Q_{1\pm}Q_{2\pm} - Q_{3\pm} > 0$ while Hopf bifurcation may occur if

$$Q_{1\pm}Q_{2\pm} - Q_{3\pm} = 0, \tag{15}$$

and $Q_{1\pm} > 0$, $Q_{3\pm} > 0$. These show that a pair of pure imaginary eigenvalues may be observed, leading to possible periodic movement.

3.3 Boundary equilibrium bifurcation

Equation (12) shows that if $w = \pm\alpha$, the admissible equilibria E_\pm collide with the pseudoequilibrium E_s at the point $E_{s\pm}(0, 0, 0)$ which are located on S^\pm . Further calculation reveals that, $f^\pm(E_{s\pm}, \pm\alpha) = 0$, but $f^\mp(E_{s\pm}, \pm\alpha) \neq 0$; $h(E_{s\pm}, \pm\alpha) = 0$; $\det(f_x^\pm(E_{s\pm}, \pm\alpha)) = \alpha(a - 1)\beta \neq 0$, i.e., $f_x^\pm(E_{s\pm}, \pm\alpha)$ is invertible; $h_w(E_{s\pm}, \pm\alpha) - h_x(E_{s\pm}, \pm\alpha) [(f_x^\pm)^{-1} f_w^\pm](E_{s\pm}, \pm\alpha) = -(1/\alpha(a - 1)) \neq 0$. Therefore, by following [27], system (3) undergoes boundary equilibrium bifurcations at $w = \pm\alpha$, with respect to fields f^+ and f^- , respectively. The type of the boundary equilibrium bifurcation will be discussed in §3.4.

3.4 Equilibrium branches and related bifurcations

Now fix the parameters at $a = 0.95$, $b = 0.1$, $\alpha = 1.82$, $\beta = 0.23$. We explore the bifurcations of equilibrium and limit cycle by regarding w as a bifurcation

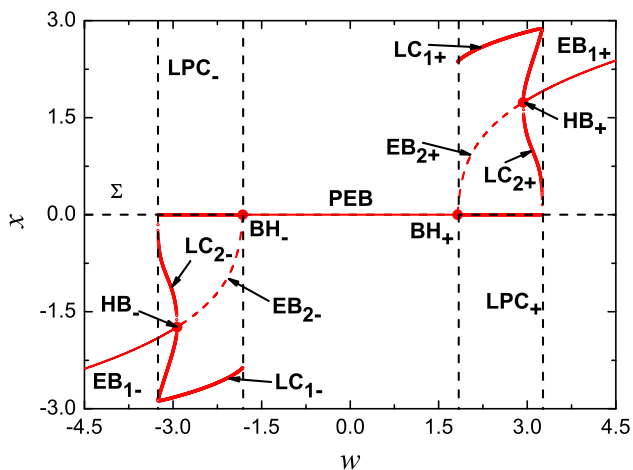


Figure 12. One-parameter bifurcation diagram with respect to w on the (w, x) plane.

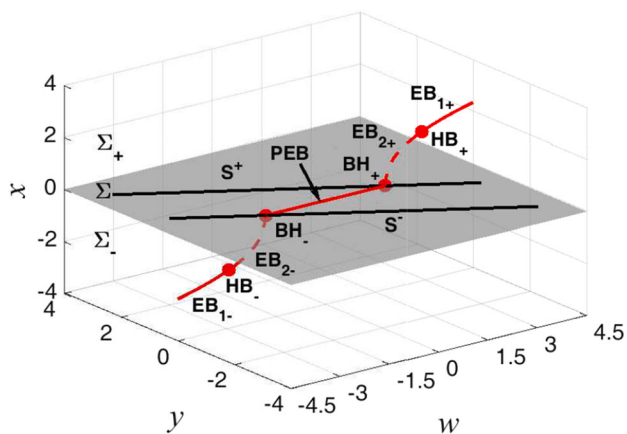


Figure 13. Equilibrium branches and the bifurcation points with respect to w, y and x , in which $BH_{\pm} \in S^{\pm}$.

parameter. One-parameter bifurcation diagram of (3) is computed numerically and projected on the (w, x) plane (see figure 12). The equilibrium branches as well as the bifurcation points with respect to w, y, x are plotted in figure 13. Meanwhile, the stability of the equilibria, the bifurcation points and the labels in the bifurcation diagram are summarised in tables 1 and 2.

In figure 12, a branch of admissible equilibria of subsystem $\dot{\mathbf{x}} = f^+(\mathbf{x}, w)$, i.e., EB_{2+} turns into a branch of pseudonodes, i.e., PEB on Σ with the decrease of w , resulting in a persistence bifurcation at BH_+ corresponding to $w = 1.82$. When $w \in (1.82, 3.254)$, there exist stable limit cycles LC_{1+} with sliding segments, seeing the representative limit cycle for $w = 2.8$ in figures 14 and 15. The periods of the limit cycles LC_{1+} drastically increase as w approaches 1.82. When $w = 1.82$, an admissible saddle collides with the pseudonode at P_2 , resulting in an orbit with infinite period

Table 1. Bifurcations, labels and critical values.

Label	Bifurcation	Critical value
BH_{\pm}	Boundary homoclinic	± 1.82
HB_{\pm}	Subcritical Hopf	± 2.92966
LPC_{\pm}	Fold limit cycle	± 3.254

Table 2. Stability of the equilibria.

Label	Stability
$EB_{1\pm}$	Stable foci
$EB_{2\pm}$	Saddles
PEB	Stable pseudonodes

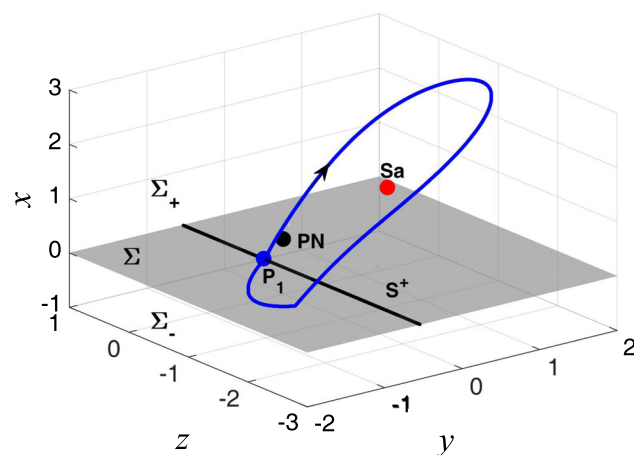


Figure 14. Representative stable limit cycle for $w = 2.8$, where PN and Sa denote the pseudonode and saddle, respectively.

(see figures 16 and 17). In this case, the boundary equilibrium bifurcation can be termed boundary homoclinic bifurcation. Because of the symmetry, another boundary homoclinic bifurcation occurs at BH_- corresponding to $w = -1.82$. Depending on the change of direction of w , the boundary homoclinic bifurcations can explain either the appearance or the disappearance of the limit cycle attractors $LC_{1\pm}$.

Subcritical Hopf bifurcations at HB_{\pm} , corresponding to $w = \pm 2.92966$, lead to the appearance of unstable limit cycles, denoted by $LC_{2\pm}$ in figure 12. $LC_{2\pm}$ are approached by the stable limit cycles $LC_{1\pm}$ as w approaches LPC_{\pm} corresponding to $w = \pm 3.254$. $LC_{1\pm}$ and $LC_{2\pm}$ coalesce and annihilate each other at $w = \pm 3.254$, resulting in the occurrence of fold limit cycle bifurcations. Notice that limit cycles $LC_{1\pm}$ involve sliding segments located on Σ (e.g., see figure 14), which means such fold limit cycle bifurcations are somewhat different from that of conventional ones, and we call them non-smooth fold limit cycle bifurcations.

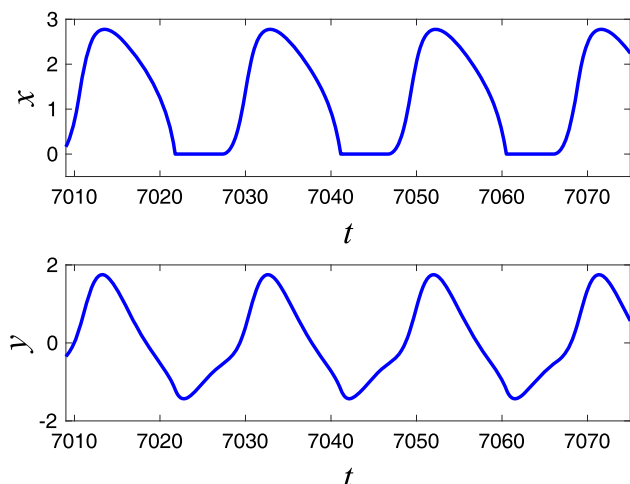


Figure 15. Time history of the limit cycle on the (t, x) plane for $w = 2.8$.

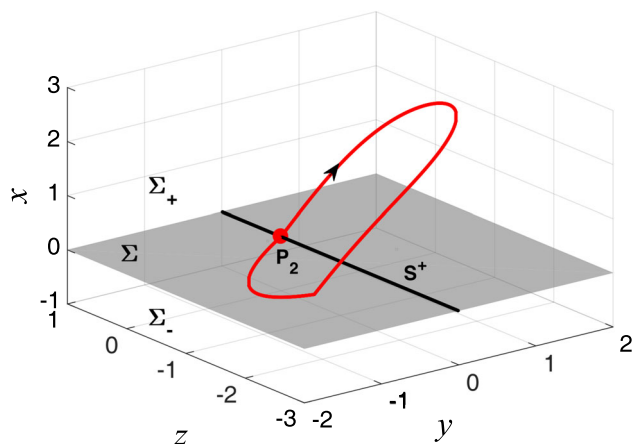


Figure 16. The boundary homoclinic orbit for $w = 1.82$.

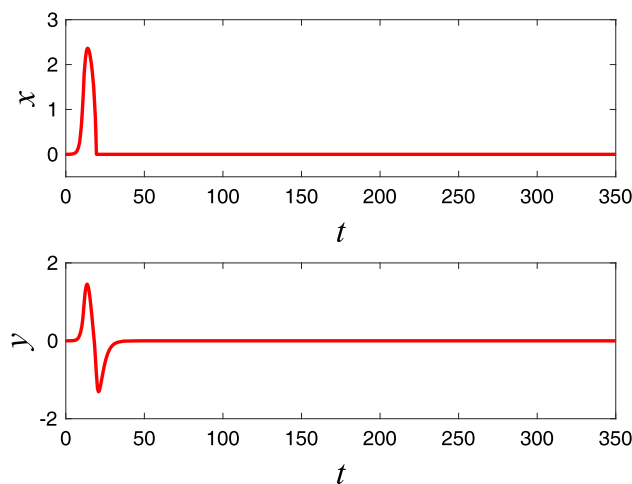


Figure 17. Time history of the boundary homoclinic orbit for $w = 1.82$.

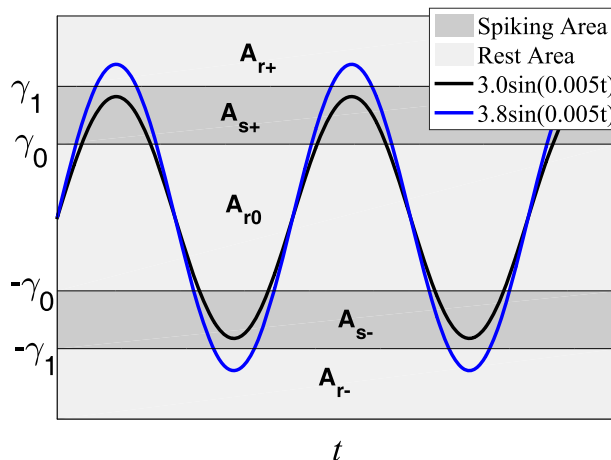


Figure 18. Rest and spiking areas: A_{r0} corresponding to a pseudoequilibrium attractor and $A_{r\pm}$ corresponding to two equilibrium attractors are the rest areas; $A_{s\pm}$ corresponding to two limit cycle attractors are the spiking areas.

4. Dynamical mechanism of bursting oscillations

In what follows, we study the dynamical mechanism of the bursting oscillations based on the bifurcation analysis in §3. In fact, the range of w can be divided into five areas by $w = \pm\gamma_0$ and $w = \pm\gamma_1$, i.e., rest areas $A_{r-} = \{w|w < -\gamma_1\}$, $A_{r0} = \{w|-\gamma_0 < w < \gamma_0\}$ and $A_{r+} = \{w|w > \gamma_1\}$, spiking areas $A_{s-} = \{w|-\gamma_1 < w < -\gamma_0\}$ and $A_{s+} = \{w|\gamma_0 < w < \gamma_1\}$ (see figure 18).

Bursting oscillations in figure 5 are formed as the external excitation slowly and periodically visits the rest area A_{r0} corresponding to a stable pseudoequilibrium attractor and the spiking areas $A_{s\pm}$ corresponding to two limit cycle attractors, while the bursting oscillations in figure 9 are formed as the external excitation slowly and periodically visits the rest areas A_{r0} , $A_{r\pm}$ and the spiking areas $A_{s\pm}$, where $A_{r\pm}$ correspond to two stable equilibrium attractors (see black and blue curves in figure 18).

We have revealed the rest and spiking areas in the range of the bifurcation parameter. Now we present the dynamical mechanism of the bursting oscillations for the two typical cases, $\gamma = 3.0$ and 3.8 .

4.1 ‘Boundary homoclinic/boundary homoclinic’ bursting

To get a clear idea of the dynamical mechanism of the bursting oscillations shown in figure 5, the transformed phase diagram of the bursting oscillations and the bifurcation diagram are overlapped with each other, which are shown in figures 19–23.

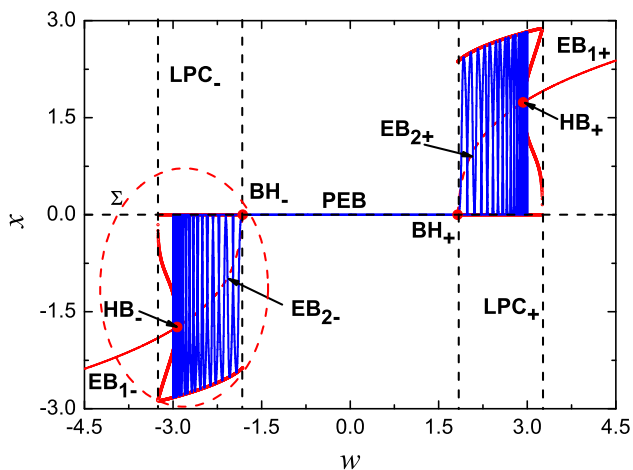


Figure 19. The overlap of the transformed phase diagram and the bifurcation diagram on the (w, x) plane for $\gamma = 3.0$.

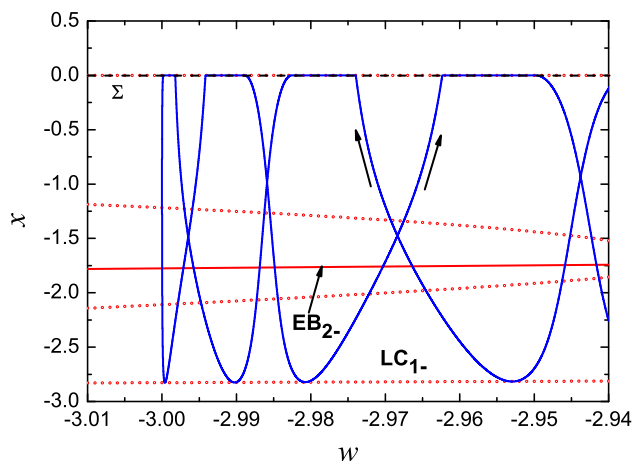


Figure 22. Locally enlarged part two of figure 20.

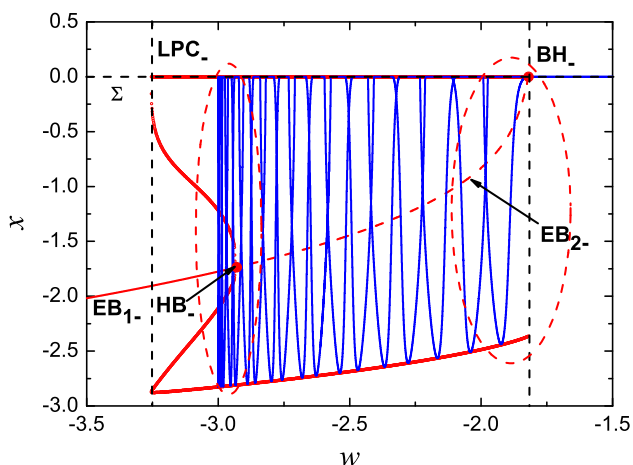


Figure 20. Locally enlarged part of figure 19.

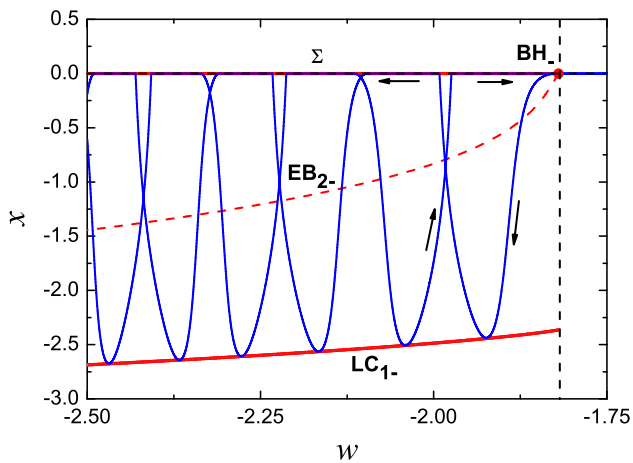


Figure 21. Locally enlarged part one of figure 20.

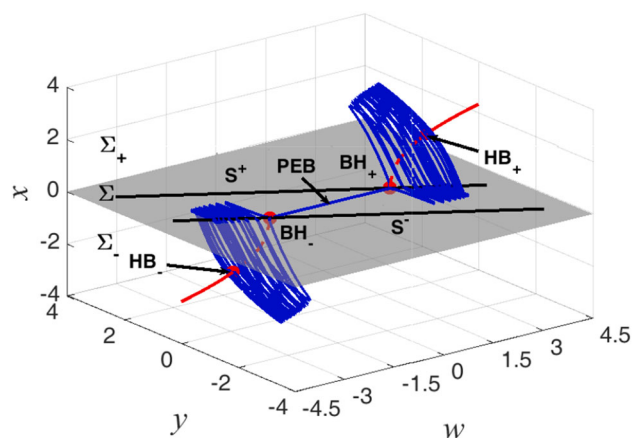


Figure 23. The transformed phase diagram and the equilibrium branch with respect to w, y and x for $\gamma = 3.0$.

Assume that the trajectory starts at the point BH_+ with $w = 1.82$, at which a boundary homoclinic bifurcation occurs (see figure 19). The system stays at the neighbourhood of the stable pseudonode of the sliding vector field in rest state until the slow-varying parameter w decreases to $w = -1.82$, corresponding to the point BH_- . Another boundary homoclinic bifurcation occurring at BH_- results in the disappearance of the rest state (see figure 20). Driven by the excitation term w , the trajectory jumps to the spiking attractor LC_{1-} and oscillates along LC_{1-} until it arrives at the minimum value of w with $w = -3.0$ (see figures 21–22). With the increase of the slow-varying variable w , the trajectory moves backward along LC_- until it arrives at the neighbourhood of the point BH_- (see figure 21). Now half period of the bursting oscillations is finished. Further increase of w leads to the other half period of the symmetric movement, which is omitted here for simplicity.

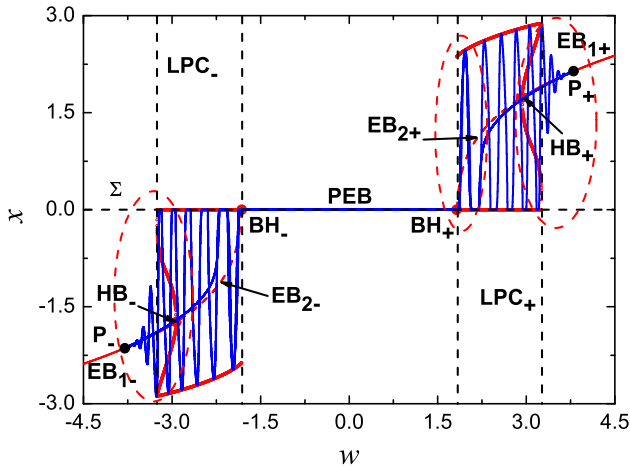


Figure 24. The overlap of the transformed phase diagram and the bifurcation diagram on the (w, x) plane for $\gamma = 3.8$.

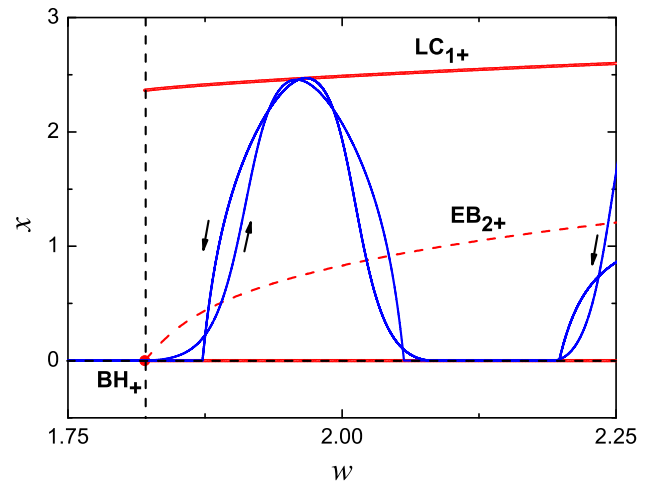


Figure 26. Locally enlarged part two of figure 24.

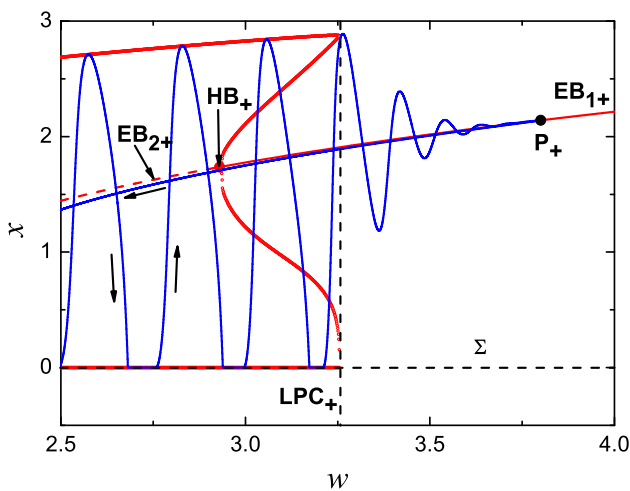


Figure 25. Locally enlarged part one of figure 24.

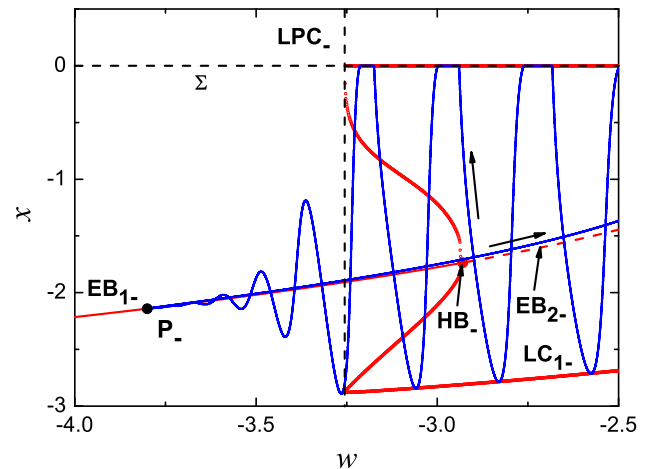


Figure 27. Locally enlarged part three of figure 24.

From the above analysis, one may find that, boundary homoclinic bifurcations lead to the transitions between the rest states and the spiking states. Therefore, this type of bursting oscillations can be called ‘boundary homoclinic/boundary homoclinic’ bursting.

4.2 ‘Boundary homoclinic/non-smooth fold cycle/sub-Hopf/boundary homoclinic’ bursting

When $\gamma = 3.8$, the subcritical Hopf and non-smooth fold limit cycle bifurcations involve the bursting attractor. The transformed phase diagram and the bifurcation diagram are overlapped in figure 24.

Assume that the trajectory starts at point P_+ corresponding to the maximum value of the slow-varying variable w with $w = 3.8$ (see figure 24). With the decrease of w , the trajectory moves along the stable focus-type equilibrium branch EB_{1+} until it arrives at

the neighbourhood of the point HB_+ , at which a subcritical Hopf bifurcation occurs (see figure 25). The instability of the saddle points on the equilibrium branch EB_{2+} causes the trajectory to leave EB_{2+} gradually. Then the trajectory is captured by the basin of attraction of the limit cycle LC_{1+} , forming a spiking state with only one peak (see figure 26). When the trajectory arrives at the neighbourhood of the point BH_+ corresponding to $w = 1.82$, a boundary homoclinic bifurcation occurs. The spiking state disappears and the system resides at the stable pseudonode of the sliding vector field in rest state until $w = -1.82$, corresponding to the point BH_- , at which another boundary homoclinic bifurcation occurs (see figure 24). The trajectory jumps to the limit cycle LC_{1-} and oscillates along LC_{1-} , until it arrives at the dash line LPC_- , corresponding to $w = -3.254$, at which a fold limit cycle bifurcation occurs (see figure 27). Attracted by the stable foci, the trajectory settles down to EB_{1-} abruptly

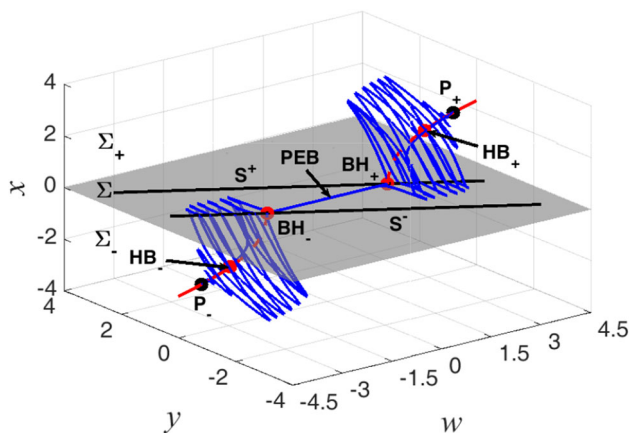


Figure 28. The transformed phase diagram and the equilibrium branch with respect to w , y and x for $\gamma = 3.8$.

and then moves along EB_{1-} until it arrives at point P_- , corresponding to the minimum value of w with $w = -3.8$ (see figure 27). Now half period of the bursting oscillations is finished. Further increase of w leads to the other half period of the symmetric movement, which is omitted here. This type of bursting oscillations can be called ‘boundary homoclinic/non-smooth fold cycle/sub-Hopf/boundary homoclinic’ bursting.

Remark 2. Once the trajectory arrives at the discontinuity boundary Σ , it will be governed by (10) and moves along the sliding region Σ^s , forming sliding solution of system (3) (see the red segments in figures 3 and 7). The sliding solution terminates at one of the sliding boundaries S^\pm or at the neighbourhood of E_0 , which is determined by the initial point where the trajectory intersects with Σ^s (see figures 23 and 28).

5. Effects of excitation amplitude and frequency on bursting oscillations

We have investigated the dynamical mechanism of bursting oscillations. In this section, we focus on the effects of external excitation amplitude and frequency on such bursting oscillations.

First, the effect of external excitation amplitude on bursting oscillations is considered. As described earlier, bursting oscillations are formed because external excitation term passes through boundary homoclinic bifurcation values $w = \gamma_0$ periodically. So, when the excitation amplitude γ satisfies $\gamma < \gamma_0$, bursting oscillations do not occur because the external excitation term is not able to pass through the boundary homoclinic

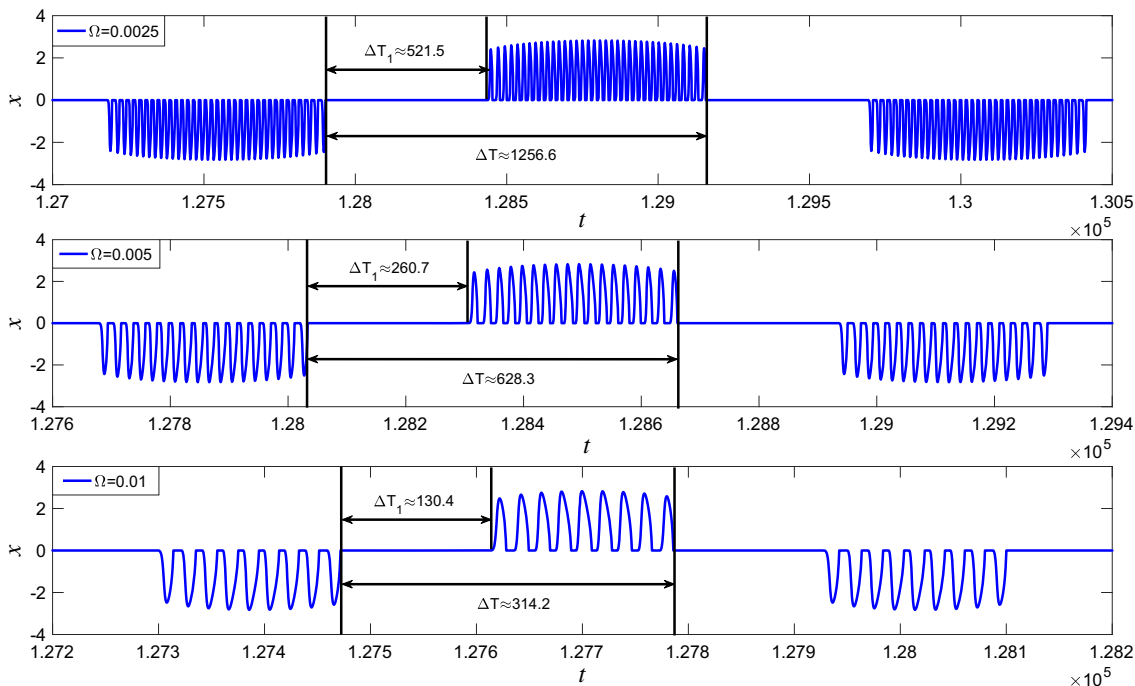


Figure 29. Numerical results of time interval between two adjacent spikes of bursting dynamics and the duration of the system staying at the stable pseudonode corresponding to figure 5 for the external excitation frequency $\omega = 0.0025, 0.005, 0.01$, respectively.

bifurcation. If $\gamma > \gamma_0$, bursting oscillations may be formed. When γ is between γ_0 and γ_1 , the dynamical mechanism of the bursting oscillations are similar to that in figures 3–5. If $\gamma > \gamma_1$, the dynamical mechanism of the bursting oscillations are similar to that in figures 7–9.

Secondly, the effect of external excitation frequency on bursting oscillations is considered. As a kind of coupling oscillator, the bursting dynamics of the whole slow–fast coupling system has the frequency of Ω . The time intervals between two symmetric adjacent spikes of bursting oscillations can be calculated, which is $\Delta T = \pi/\Omega$. Furthermore, the duration of the system staying at the stable pseudonode is concluded at $\Delta T_1 = (2/\Omega) \arcsin(\alpha/\gamma)$. When $\Omega = 0.0025, 0.005$ and 0.01 , we have $\Delta T = 400\pi, 200\pi$ and 100π , respectively. Take the waveforms in figure 5 as an example, when $\Omega = 0.0025, 0.005$ and 0.01 respectively, the corresponding time intervals ΔT_1 and ΔT are measured and shown in figure 29, where the numerical results agree well with the analytical ones.

6. Conclusion

Because of non-smoothness, a Chua's circuit of Filippov-type may exhibit bursting oscillations with new patterns under certain external excitation conditions. Uncovering the essence of the bursting oscillations is an important issue in non-smooth bursting dynamics. We first consider the external excitation term as a bifurcation parameter and study its influence on the generalised autonomous system, and at the same time, we explore the sliding solution of the Filippov system and pseudoequilibrium bifurcation of the sliding vector field on the switching manifold. Then employ the transformed phase diagram to account for the bursting oscillations. Boundary homoclinic bifurcation, non-smooth fold limit cycle bifurcation and subcritical Hopf bifurcation may result in the system's switching between different attractors, forming complicated bursting oscillations, which shows that the transitions between rest states and spiking states may be caused by not only the conventional bifurcations but also the non-smooth bifurcations. Here, we would like to suggest that the dynamical behaviours of the system on the switching manifold should be considered, as the sliding vector field on the switching manifold may influence the bursting attractor of a Filippov systems. Our research enriches the non-smooth dynamics of the bursting oscillations in the Filippov system.

Acknowledgements

This work was supported by the National Natural Science Foundation of China (Grant Nos 11632008, 11872189).

References

- [1] Z Rakaric and I Kovacic, *Mech. Syst. Signal Pr.* **81**, 35 (2016)
- [2] T Hayashi, *Phys. Rev. Lett.* **84**, 3334 (2000)
- [3] V K Vanag, L Yang and M Dolnik, *Nature* **406**, 389 (2000)
- [4] O Decroly and A Goldbeter, *J. Theor. Biol.* **124**, 219 (1987)
- [5] P Bressloff and S Coombes, *Neural Comput.* **12**, 91 (2000)
- [6] M Beierlein, J Gibson and B Connors, *J. Neurophysiol.* **90**, 2987 (2003)
- [7] E Brown, J Moehlis and P Holmes, *Neural Comput.* **16**, 673 (2004)
- [8] J Rinzel, Bursting oscillations in an excitable membrane model, in: *Ordinary and partial differential equations* edited by B D Sleeman and R J Jarvis (Springer, Berlin, Heidelberg, 1985)
- [9] E Izhikevich, *Int. J. Bifurc. Chaos* **10**, 1171 (2000)
- [10] X J Han and Q S Bi, *Commun. Nonlinear Sci.* **16**, 4146 (2011)
- [11] I Kovacic, M Cartmell and M Zukovic, *Proc. R. Soc. A* **471**, 20150638 (2015)
- [12] Z D Zhang, B B Liu and Q S Bi, *Nonlinear Dyn.* **79**, 195 (2015)
- [13] Q S Bi, X K Chen, J Kurths and Z D Zhang, *Nonlinear Dyn.* **85**, 2233 (2016)
- [14] X J Han, Y Yu, C Zhang, F B Xia and Q S Bi, *Int. J. Nonlinear Mech.* **89**, 69 (2017)
- [15] Z X Wang, Z D Zhang and Q S Bi, *Int. J. Bifurc. Chaos* **29**, 1930019 (2019)
- [16] M Jeffrey, *Physica D* **241**, 2077 (2012)
- [17] R Qu, Y Wang, G Q Wu, Z D Zhang and Q S Bi, *Int. J. Bifurc. Chaos* **28**, 1850146 (2018)
- [18] Z F Qu, Z D Zhang, M Peng and Q S Bi, *Pramana – J. Phys.* **91**: 72 (2018)
- [19] T Singla, T Sinha and P Parmananda, *Chaos Solitons Fractals* **75**, 212 (2015)
- [20] T C Lin, F Y Huang, Z b Du and Y C Lin, *Int. J. Fuzzy Syst.* **17**, 206 (2015)
- [21] K Rajagopal, S Kacar, Z C Wei, P Duraisamy, T Kifle and A Karthikeyan, *Int. J. Electron. Commun. (AEÜ)* **107**, 183 (2019)
- [22] Er V Kal'yanov and B E Kyarginiskiĭ, *Tech. Phys. Lett.* **32**, 35 (2006)
- [23] H Mkaouar and O Boubaker, *Pramana – J. Phys.* **88**: 9 (2017)
- [24] Q S Bi, S L Li, J Kurths and Z D Zhang, *Nonlinear Dyn.* **85**, 993 (2016)

- [25] R Cristiano, T Carvalho, D J Tonon and D J Pagano, *Physica D* **347**, 12 (2017)
- [26] A F Filippov, Differential equations with discontinuous right-hand sides, in: *Mathematics and its applications (Soviet Series)* edited by F M Arscott (Springer, Dordrecht, 1988)
- [27] M di Bernardo, C J Budd, A R Champneys and P Kowalczyk, Piecewise-smooth dynamical systems: Theory and applications, in: *Applied mathematical sciences* edited by S Antman, J Marsden and L Sirovich (Springer, London, 2008)